ANALYSIS OF Pc3 AND Pc4 GEOMAGNETIC PULSATIONS OVER THE AMAZON REGION

Sebastião Wendell Nobres Moura [ID][1], Raphael Di Carlo Silva dos Santos [ID][2]*,
Giorgio Arlan da Silva Picanço [ID][3], Mayara Fraeda Barbosa Teixeira [ID][2],
and Jean Ricardo Mesquita Machado [ID][4]

[1] Universidade Federal do Oeste do Pará - UFOPA, Instituto de Engenharia e Geociências, Santarém, PA, Brazil
[2] Universidade Federal do Amazonas - UFAM, Instituto de Ciências Exatas, Manaus, AM, Brazil
[3] Instituto Nacional de Pesquisas Espaciais, Divisão de Aeronomia, São José dos Campos, SP, Brazil
[4] Universidade Federal do Pará - UFPA, Instituto de Geociências, Belém, PA, Brazil

*Corresponding author email: raphaelsantos@ufam.edu.br

ABSTRACT. The geomagnetic field produces aeronomic phenomena according to the Earth's magnetic latitude. In South America, we find two important phenomena: the South America Magnetic Anomaly (SAMA) and the Equatorial Electrojet (EEJ). This study aimed to analyze the amplitudes of continuous magnetic pulsations (Pc3 and Pc4 type) in magnetic stations located between EEJ and SAMA. Based on the Dst index, we acquired data from four monitoring stations on quiet and disturbed days in August 2018. The magnetic pulsations in the equatorial region are related to the type of ionospheric conductivity, such as Cowling's conductivity, contributing to amplifying the damping of Pcs wavelength. Finally, we found evidence that suggests a potential influence of the EEJ behavior on the amplitudes of Pc3 and Pc4. Therefore, the present study contributes to future research to fully understand the nature and extent of this influence.

Keywords: geomagnetic field; aeronomy; geomagnetism; Amazon region.

INTRODUCTION

Geomagnetic pulsations are low-frequency magnetospheric disturbances driven by the effects of solar wind interactions (Hasegawa and Chen, 1974). These phenomena are usually generated by magnetohydrodynamic waves, which result from the interaction between a fluid with high electrical conductivity and a magnetic field. In the solar-terrestrial environment, these pulsations typically occur in the ultralow frequencies (ULF) band, and their origin can derive from several processes and instabilities of the solar plasma, along with Earth's Magnetic Field (EMF) variations (McPherron, 2005). In this way, geomagnetic pulsations can be classified into two main types: irregular (Pi) and continuous pulsations (Pc) (Saito, 1969). Generally, observations of pulsations are used for studying the Earth's magnetic field temporal behavior, and its classification can also be done according to the wave period and morphology (Jacobs et al., 1964).

Among the main phenomena that affect the EMF, the South America Magnetic Anomaly (SAMA) plays a significant role in the geomagnetic pulsation mechanism. In short, the geomagnetic field weakening over the SAMA region can affect some local aeronomic phenomena, such as the dynamic of ionospheric irregularities (Chapman and Bartels, 1940; Campbell, 2003). On the other hand, the EMF intensity can also be affected by the Equatorial Electrojet (EEJ), which is defined as the electric current that flows in the ionospheric E-region during the daytime, when the highest EMF values occur (Sarma and Sastry, 1995; Kelley, 2009; Silva, 2017). In this regard, many studies indicate that the amplification or attenuation of certain types of geomagnetic pulsations can be related to changes in the EEJ intensity, due to the increased/decreased Cowling conductivity in its region of influence. However, the influence of the EEJ on geomagnetic pulsations during different solar cycle stages is an open topic of investigation. For instance, Silva (2017) states that the geomagnetic pulsations are generally amplified under the EEJ zone, as the Pc4 (wave period: 45s) and Pc5 (wave period: 600s) signals usually start to increase in relation to the region outside the EEJ influence (±3 to ±10 degrees MLAT; Patra and Rao, 2006). Furthermore, Shinohara et al. (1998) suggest that the signals are generally attenuated at the intervals belonging to Pc3 at the magnetic equator. However, it is relevant to mention that the cause for different observations found at the

magnetic equator has not yet been a unified answer in the literature. Recent theories indicate that the effects on the pulsation amplitudes are associated with the Cowling conductivity characteristics (Kikuchi and Araki, 1979; Itonaga et al., 1998).

To better understand these phenomena, this study aims to identify and evaluate Pc3 and Pc4 signals in and around the Amazon Region. For that, we used data from several stations with different magnetic latitudes. Specifically, we used data obtained in August 2018 from magnetic stations located near the magnetic equator, such as Tatuoca and Araguatins (Brazil), Kourou (French Guiana), and San Juan (Puerto Rico). Finally, we performed a spectral analysis to identify the Pc3 and Pc4 pulsations using bandpass filters and spectrograms of the EMF horizontal component values.

SOLAR-TERRESTRIAL ENVIRONMENT AND GEOMAGNETIC PULSATIONS

The Sun has an activity cycle of approximately 11 years, characterized by variations in the number of Sunspots. Besides its variable activity, the Sun is also a continuous source of plasma flowing in the interplanetary medium: the solar wind (Parks, 1991; Schunk and Nagy, 2009). The solar wind leaves the Sun with a velocity of between 300 km/s and 800 km/s, depending on the Sun's activity, and frequently occurs towards the Earth's magnetosphere (Marchezi, 2016). Thus, due to its capacity to interact with the Earth's magnetosphere, the solar wind is the leading cause of several planetary disturbances within the solar-terrestrial environment (Biermann, 1963; Parks, 1991; Kivelson and Russell, 1995).

Furthermore, the plasma that makes up the solar wind is highly conductive and carries Interplanetary Magnetic Field (IMF) 'frozen' lines. These field lines follow the Sun's rotation, which occurs over approximately 27 days, configuring a field geometry in a spiral shape and generating an angle of ~45° in relation to the Sun-Earth axis. In addition, coronal mass ejections (CME) are sporadic discharges of plasma with high density and velocity. When traveling toward Earth, CMEs can be the primary source of energy for several aeronomic phenomena (Kivelson and Russell, 1995; Moldwin, 2008).

Inside the magnetosphere, we find four zones where geomagnetic pulsation amplitudes can be measured: the magnetotail—the night side of the magnetosphere; the plasmasphere—the inner region of the magnetosphere which is parallel with the Earth's axis of rotation and where the densest plasma of electrical particles is found; the plasma sheet—location with a flow of intense and unstable electrical current; and the Van Allen Belt—characterized by the presence of charged and trapped particles in the geomagnetic field (Silva, 2017). The solar wind compresses the magnetosphere on the dayside and along the magnetospheric tail on the nightside. At moments of high solar wind ejection, the plasma compresses the magnetosphere towards Earth, and the magnetotail starts to stretch. This high plasma ejection interacts with the electrical current systems of the ionosphere, causing magnetic disturbances.

The geomagnetic disturbances can be expressed by the magnetohydrodynamic wave equations, which describe the interaction between magnetic field lines and fluids of high electrical conductivity (Dungey, 1961). Thus, it is reasonable to state that the geomagnetic pulsations observed on Earth's surface are an effect of the magnetohydrodynamic waves generated in the interplanetary environment (Kivelson and Russell, 1995; McPherron, 2005). Moreover, the disturbances of the EMF may be observed on different time scales, from seconds to millions of years. The slow variations are caused by the outer core dynamics, as the fast variations are associated with the magnetosphere dynamics caused by the interaction with the solar plasma. The magnetic disturbances are classified as "secular" for events that last longer than one year, "daily" for periods longer than 24 hours, "disturbs" for events associated with magnetic storms, "pulsations" for periods between 0.2 and 100 seconds, and "atmospherical" for periods less than 1 second (Saito, 1969).

The geomagnetic pulsations are associated with the ultralow frequencies (ULF) of the magnetosphere. The range of these frequencies varies from 1 mHz to 10 Hz, and their amplitudes are higher than 100 nT (Saito, 1969). We can divide the pulsations into three distinct frequency bands: low (1-10 Hz), medium (10-100 mHz), and high (0.1-10 Hz). The irregular pulsations are comparatively shorter in duration and are generally composed of a few oscillations decaying in time, presenting a sinusoidal shape or well-defined spectral peak. The continuous pulsations cover the period interval from 0.2 to 600 seconds.

The H+ cyclotron frequency is ~10 Hz in the magnetosphere, which is the upper limit for geomagnetic pulsations (Samson, 1991; Sibeck, 1994). The lower limit, ~1 mHz, is characterized by its propagation time through the magnetosphere (Kamide and Chian, 2007). Pc4 pulsations are low-frequency plasma waves with wavelengths comparable to the dimensions of the magnetosphere (Samson, 1991). These pulsations commonly have two peaks of amplitudes: one near the aurora zone and the other in the sub-auroral region. At medium latitudes, the pulsation occurrence is maximum at local noon (Saito, 1969), and they are caused predominantly by phenomena such as the Kelvin-Helmholtz's instability. The Pc3 pulses are generated by the impact of the solar wind at the magnetopause. In this context, plasma waves generated by these instabilities generally move from the bow shock to the magnetopause and the inner magnetosphere. In addition, they occur frequently at dawn, with periods varying and maximizing at noon (Samson, 1991; Murphy and Egbert, 2018; Heyns et al., 2020; Chen et al., 2021; Yagova et al., 2021; Omondi et al., 2022).

METHODOLOGY

Classification of Geomagnetic Pulsations

Table 1 shows a classification of the geomagnetic pulsations according to their periods.

Table 1 - Classification of geomagnetic pulsations according to their periods. Adapted from Jacobs et al. (1964).

Pulse	Period interval (s)	Frequency interval
Pc1	0.2 – 5.0	0.2-5 Hz
Pc2	5.0 – 10.0	0.1-0.2 Hz
Pc3	10.0 – 45.0	22 – 100 mHz
Pc4	45.0 – 150.0	7 – 22 mHz
Pc5	150.0 – 600.0	2 – 7 mHz
Pi1	1.0 – 40.0	0.025 – 1 Hz
Pi2	40.0 – 150.0	2 – 25 mHz

The Dst index

The Disturbance Storm Time (Dst) index is a relative equatorial measure of the current that flows into the Van Allen radiation belt, known as the ring current (Aarons, 1991). The intensities of geomagnetic storms can be classified according to this index (Gonzalez et al., 1994). Geomagnetic storms can be divided into three phases according to the behavior of the Dst. The initial phase is preceded (or not) by a sudden commencement, lasting for some minutes to a few hours and with an increase in the index to a few hundred nanoteslas. The main phase is characterized by a decrease in the index value, reaching hundreds of negative nanoteslas. And the recovery phase, when the index starts to show undisturbed values, indicates the end of the storm. The end of the recovery phase is identified when the Dst reaches a value equal to 1/10 of the minimum value observed during the storm main phase (Gonzalez et al., 1994).

Data acquisition

We chose the data using the following criteria: (i) availability, (ii) location, (iii) sampling rate, and (iv) Dst index intensity. The data which fulfilled all criteria were from August 2018. At the end of the month, we identified a magnetic storm that started on

26 August 2018 and ended on 31 August 2018. In this study, we acquired the horizontal component H of the magnetic data defined as:

$$H = \sqrt{H_x^2 + H_y^2}, \qquad (1)$$

where Hx and Hy are the values of the geomagnetic field in north and east coordinates, respectively. We used data from the stations of San Juan (SJG), Kourou (KOU), Araguatins (ARA), and Tatuoca (TTB). They were acquired from the worldwide network of magnetometers, INTERMAGNET, through acquisitions from the German Geoscience Research Center (GFZ) and the Brazilian Magnetometer Network (EMBRACE) (Denardini et al., 2018). The data from Tatuoca were acquired by the National Observatory (ON) team responsible for the operation of the station.

The furthest station to the magnetic equator is San Juan, in Puerto Rico, with a latitude and longitude corresponding to 18.45º and −66.06º, respectively. Its elevation is 424m. The institute responsible for its operation is the United States Geological Survey (USA). Kourou station, located in French Guiana, is very close to the magnetic equator during the period of study. It is located at 5.14º and −52.65º with an elevation of 10 m and is administrated by the Institut de Physique du Globe (France). The Tatuoca station is the closest station to the magnetic equator, located at -1.50º and -48.50º, in Pará state, with an elevation of 10m, and is maintained by the German Geoscience Research Center and National Observatory (ON). Finally, the Araguatins station, located at -5.60º and -48.10º in Tocantins state with an elevation of 103m, is coordinated by the National Observatory.

Table 2 lists the latitude, longitude, dip angle, magnetic field strength (B), and elevation of each station.

We chose the dates with intense solar activity, as measured by Kyoto Observatory; therefore, we analyzed the global mean of the EMF intensity. Figure 1 shows the Dst index for the period from 20 to 28 August 2018, where we find a magnetic storm signature at the day 25. The period from 21 to 23 is characterized as quiet days while the days 25, 26 to 27 represent disturbed days. Higher amplitudes are noticeable during this period, indicating the impact of the storm on the magnetic field.

Table 2 - List of the stations used in this study, along with their geographic coordinates, dip angles, total magnetic field strength (B) in nanotesla (nT), and elevation in meters above sea level.

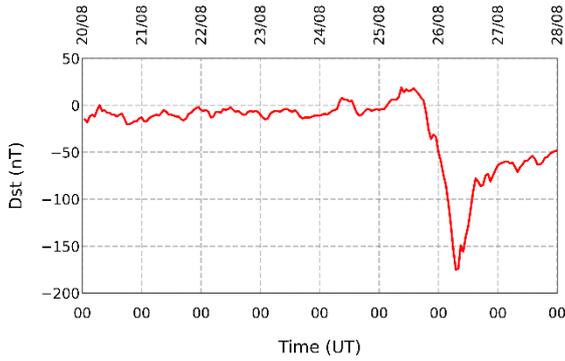| Station (Code)	Latitude (°)	Longitude (°)	Dip (°)	B (nT)	Elev. (m)
San Juan (SJG)	18.45	-66.06	43.06	30341	424
Kourou (KOU)	5.14	-52.65	13.69	28532	10
Tatuoca (TTB)	-1.20	-48.10	-2.60	26281	10
Araguatins (ARA)	-5.60	-48.10	-10.62	24059	103

Figure 1: Dst index time variation for the period from 20 to 28 August 2018.

We chose the stations based on their proximity to the EEJ region so that we could investigate how the intensity of the EEJ electric current flow affects Pc pulse identification. SJG is the only station outside the EEJ region because we intended to verify if the ionospheric current flow significantly attenuates or accentuates the pulse identification in this region. Figure 2 shows a map with the geographic locations of the magnetic stations used in this study. This map also includes the isolines of magnetic inclinations calculated using the IGRF-13 (International Geomagnetic Reference Field) magnetic model (Alken et al., 2021).

Data filtering

The frequencies related to Pc3 and Pc4 pulses were mapped using a time series filtering of the H component and calculating its dynamic spectrum, producing a frequency spectrogram. The time series is classified as a group of data points listed on a time scale, not strictly following an equally spaced sequence (Kanasewich, 1981). We used a Butterworth bandpass digital filter type with the frequencies limited to the Pc3 and Pc4 pulses. These digital filters derive from functions that perform temporal analysis and provide a signal with a frequency previously specified.

To identify both pulses, we performed a Fourier transform (FT) of the H component expressed as:

$$F(\omega) = \int_0^T f(t)e^{-i\omega t}dt, \qquad (2)$$

where $f(t)$ is the H component in the function of time, T is the period of the signal, and ω is the angular frequency denoted by $\omega = 2\pi/T$. The Fourier transform is applied only on stationary signals; however, the geomagnetic field is a function of time and space. To perform the FT on non-stationary signals, it is necessary to incorporate the time variation effect, so we apply the Short-Time Fourier transform (STFT) instead. The STFT divides a longer time signal into shorter windows of the same length and calculates the FT on each window separately. First, it calculates the discrete FT on a window with M elements $(f_1, f_2, \ldots, f_{M-1})$, then it moves the window using a constant time interval and calculates the FT

in the window $(f_1, f_2, \ldots, f_M)$. The procedure is repeated until the window covers the last N points of the input data and calculates the FT in the window $(f_{N-M}, \ldots, f_{N-1})$ (Okamura, 2011). The STFT is expressed as:

$$F(\sigma, \omega) = \int_{-\infty}^{\infty} f(t)W(t-\sigma)e^{-i\omega t}dt, \qquad (3)$$

where $W(\sigma)$ is the window function, and σ is the time index. The output of equation (3) evaluation is the spectrogram.
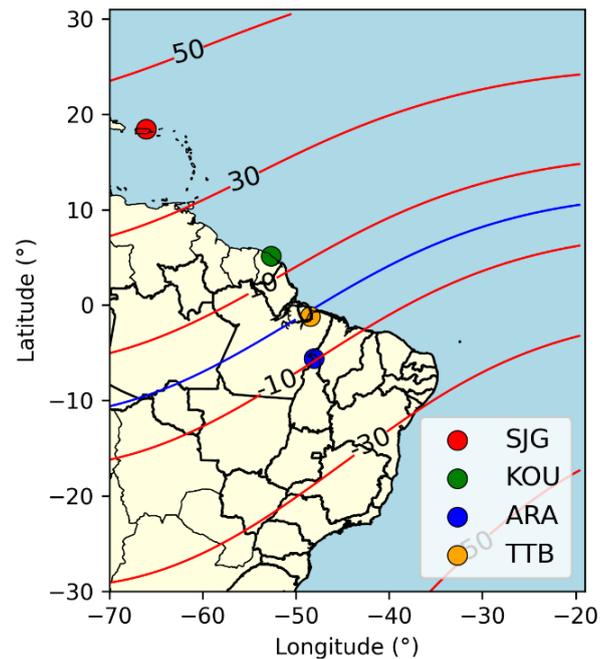

Figure 2: Geographical distribution of the geomagnetic stations used in the study and isolines of magnetic inclination calculated using the IGRF-13 magnetic model.

We divided the data into two groups: geomagnetic quiet and disturbed days. To identify the correct signal of the Pcs, we adopted Piassi´s criteria (2018): (a) Pc3 must have a minimum amplitude of 0.1 nT, and Pc4 must have a minimum amplitude of 0.2 nT; (b) the amplitudes must present the same waveform in all stations and (c) minimum period of 3 wave cycles for both Pcs signal.

RESULTS

To identify the geomagnetic pulsations, we analyzed data from 21, 22, and 23 (quiet days), 25, 26 and 27 (disturbed days) August 2018. For that, we analyzed the dB/Hz ratio of the signals, which represents the power spectral density (PSD) of a given signal in decibels per hertz (Youngworth et al., 2005). Therefore, this parameter represents the amount of power contained in the signal per unit of frequency and can show how much of the signal is composed of contributions from geomagnetic pulsations. We did

not find data for the station ARA for the quiet days. The pulsations are shown in UT (universal time), which is approximately 3 hours later than the local time (LT) of the stations.

Identification of Pc3 geomagnetic pulses

For quiet days we found eight pulses in total indicating a Pc3 in KOU, ARA, and TTB stations on days 21, 22, and 23 August 2018. We did not find data from TTB on day 22, though. These pulses were found on days 21 and 22, but day 23 did not show any significant pulse that filled Piassi´s criteria (2018). Figure 3 shows two pulses for each station (red rectangle) on day 21, and Figure 4 shows one pulse (red rectangle) for each station on day 22 with amplitudes greater than 0.1nT. A possible explanation for this may be associated with the emission of charged particles from the Sun, which promotes momentary variations in the intensity of the Earth's magnetic field. However, a more in-depth study should be conducted to understand the source of these disturbances.

For disturbed days, we found nine pulses in total from day 26 to 27 August 2018. We did not find any event on day 25 which could be identified as a pulse according to Piassi´s criteria (2018). On day 26, the Dst index showed the lower value for the period: -198 nT. Figure 5 shows two pulses at KOU station (two red rectangles), two pulses at SJG station (two red rectangles) and two pulses at ARA station (two red rectangles) on day 26. Figure 6 shows one pulse at KOU station (red rectangle), one pulse at SJG station (red rectangle) and one pulse at ARA station (red rectangle) on day 27. Figure 5 shows the first Pc3 pulses between 07:00 UT and 08:00 UT, which may be related to the geomagnetic storm of day 26 and the influence of EEJ. The other pulses were found

between 17:00 UT and 18:00 UT. In this context, it is suggested that the increase of Pc3 during disturbed days can be directly related to the quantity of solar matter flowing toward the Earth's magnetic field. However, to further clarify the relationship between solar matter and geomagnetic disturbances, a more detailed investigation of the solar particle flux is required. The circles in Figure 5 evidence two pulses; however, they do not show any pulse at the same time for SJG, so we do not consider them Pc3 pulses. On the other hand, the red rectangles point out signals as probable Pc3 pulses because they fill the criteria. SJG presents pulses with low intensity compared to the other stations.

Figure 6 illustrates fewer pulses than on day 26 because the EMF is about to start the recovery phase of the geomagnetic storm. Figure 7 shows the spectrogram of day 26 between 07:50 UT and 08:50 UT, presenting a high spectral density power in the Pc3 zones. There are no data for TTB all day for day 26, so we acquired data just for the interval between 07:50 UT and 08:50 UT and between 17:00 UT and 18:00 UT. This could be explained because SJG is distant from the magnetic equator, so the effects of EEJ influence the other stations even in the recovery phase. Figure 8 shows the spectrogram of day 26 between 17:00 UT and 18:00 UT, presenting a high dB/Hz ratio in the Pc3 zones.

Figure 9 displays the spectrogram for the SJG, KOU, and ARA stations on day 27. There are no data for TTB on 27 August 2018. An evident pulse is observed simultaneously across all stations. However, it is noteworthy that the pulse exhibits higher amplitudes at the ARA station compared to those at the KOU and SJG stations. This phenomenon can be attributed to the proximity of the ARA station to the EEJ zone relative to the other stations. Therefore, it is reasonable to state that in this instance, pulse amplitude correlates with the EEJ current.
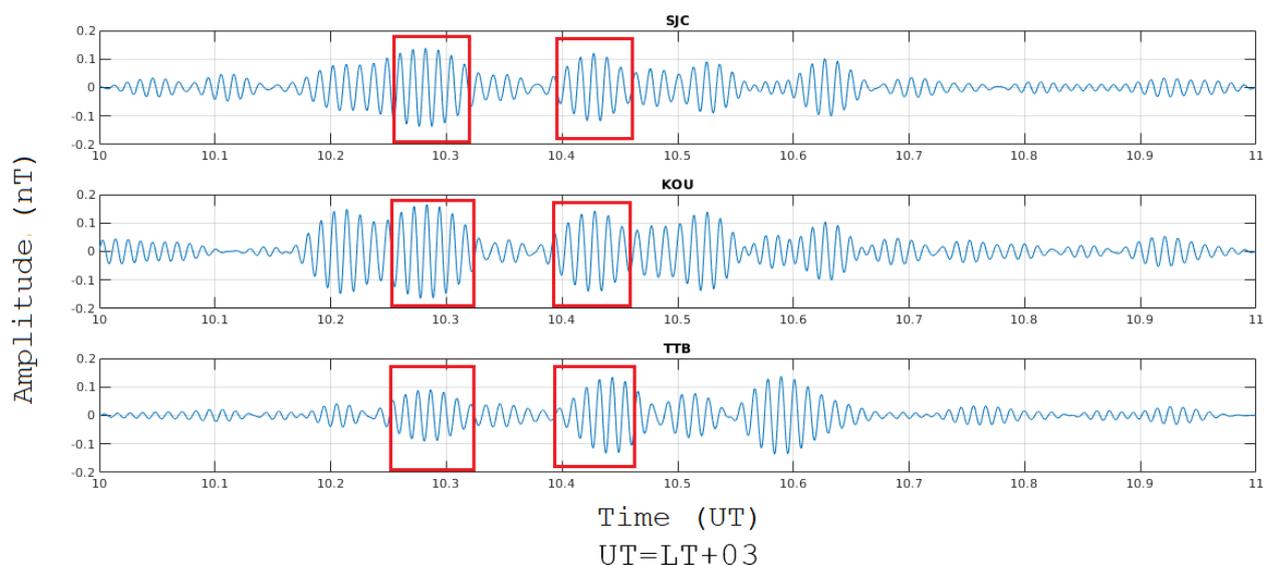

Figure 3: Identification of Pc3 pulsations of KOU, TTB, and SJG stations on 21 August 2018. Red rectangles identify the pulses.
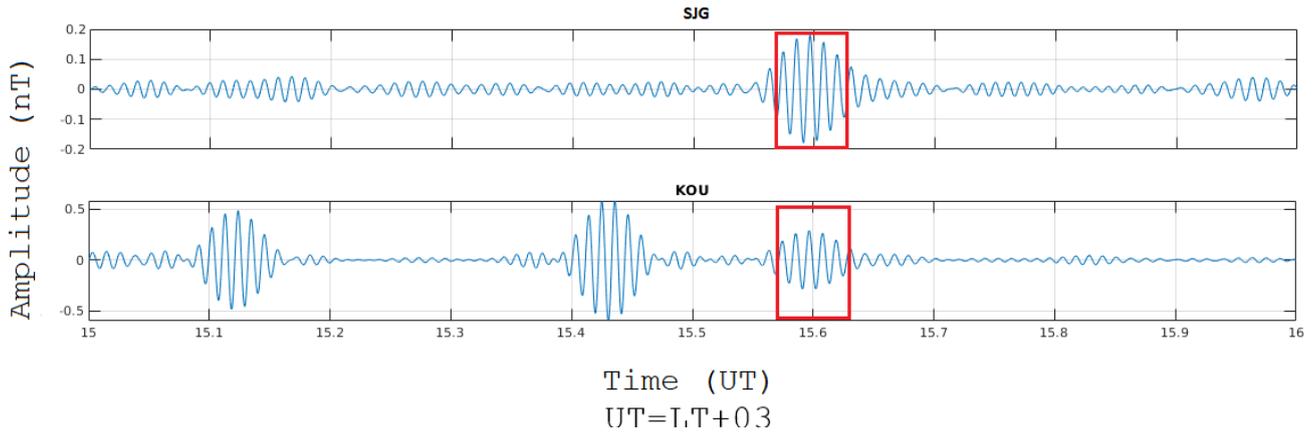
Figure 4: Identification of Pc3 pulses of KOU and SJG stations on 22 August 2018. Red rectangles identify the pulses.
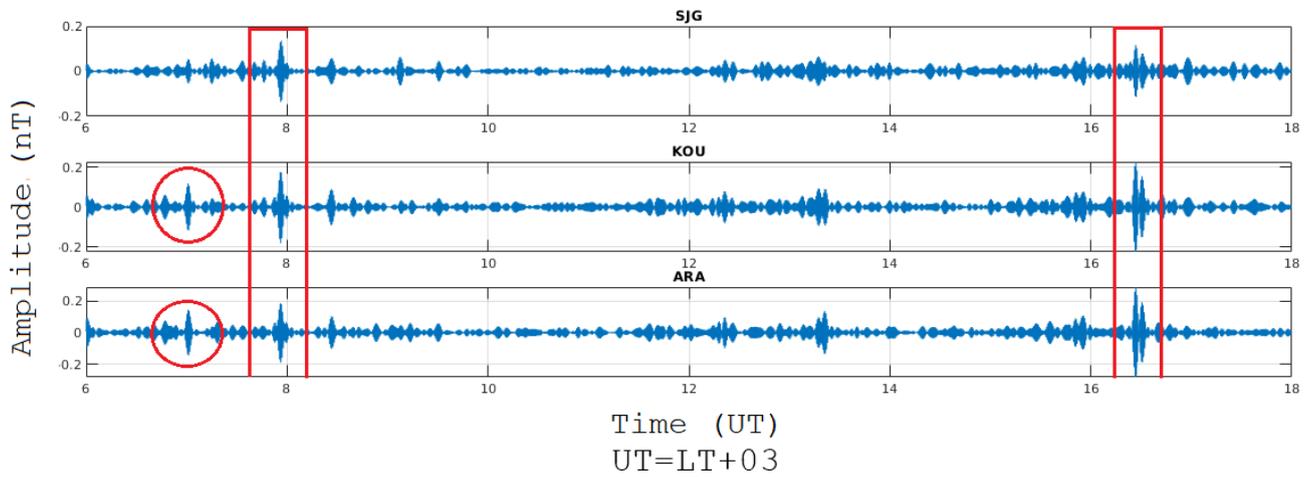

Figure 5: Pc3 identification on 26 August 2018. Red rectangles identify the pulses and circles point to signals which appear to be a Pc3 pulse.
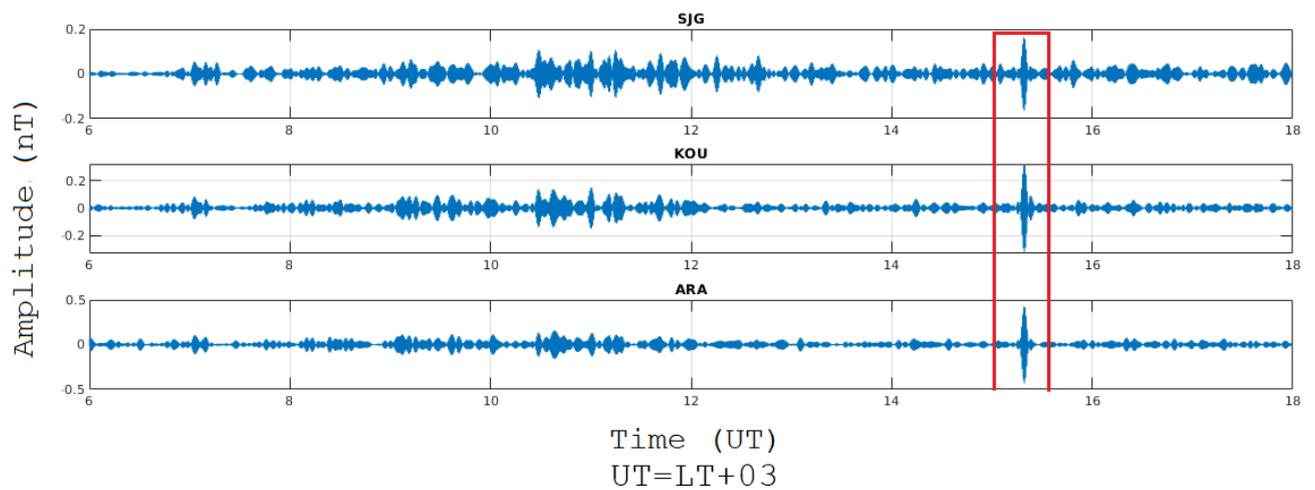

Figure 6: Pc3 identification on 27 August 2018. Red rectangles identify the pulses.
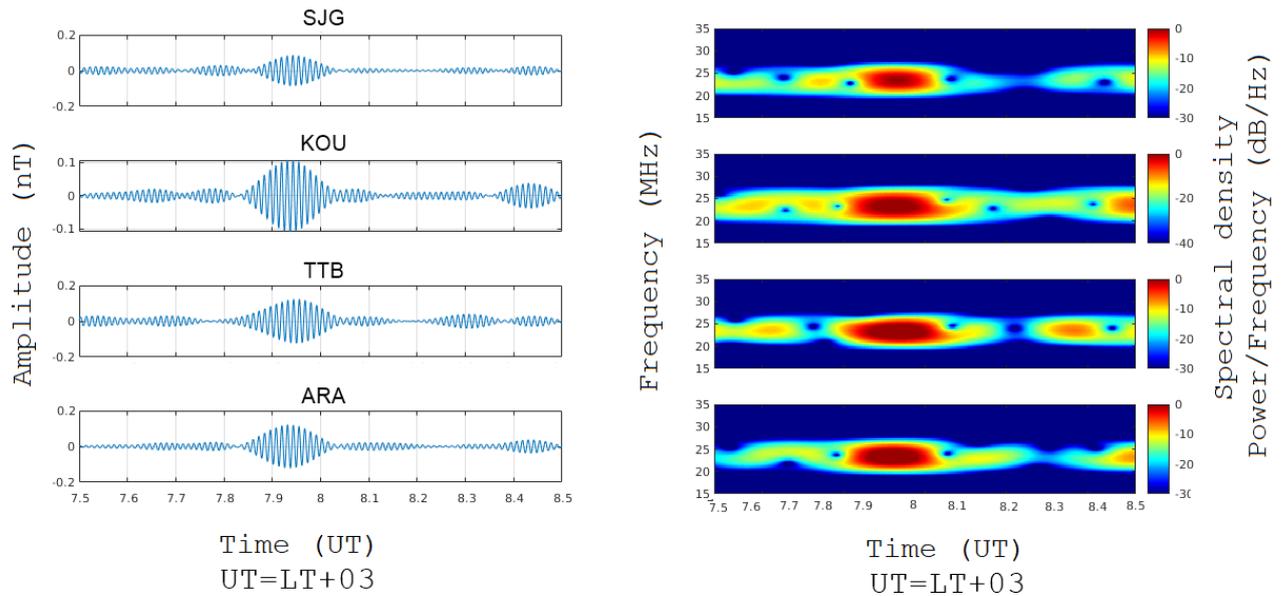
Figure 7: Identification of Pc3 pulsations of KOU, TTB, SJG, and ARA stations on 26 August 2018 from 07:50 UT to 08:50 UT. Left: pulsation amplitudes. Right: pulsation spectrograms.
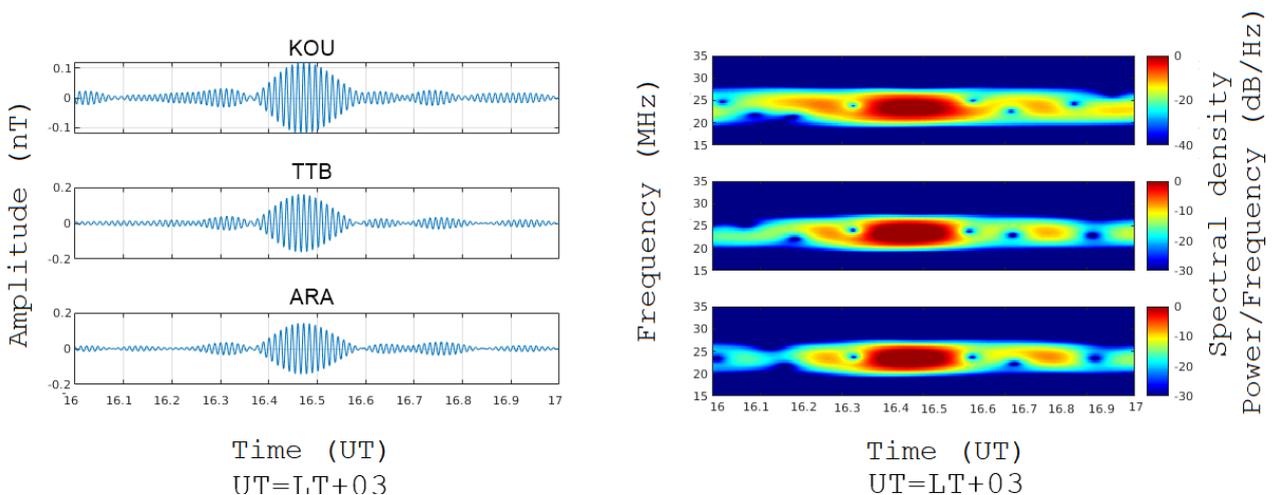
Figure 8: Identification of Pc3 pulsations of KOU, TTB, SJG, and ARA stations on 26 August 2018 from 16:00 UT to 17:00 UT. Left: pulse amplitudes. Right: pulse spectrograms.

Identification of Pc4 geomagnetic pulses

We found two pulses for quiet days on days 21, 22, and 23 August 2018. Only day 21 showed Pc4 pulses (red rectangles in Figure 10), one pulse at KOU station and one pulse at SJG station, filling the criteria. Also, there is one pulse identified at TTB station but there are no data during the entire day. Plus, there are no data from TTB on days 22 and 23 and from ARA on all three days. The pulses presented a smooth increase in their amplitudes in function of the proximity of the EEJ zone. In this context, Yagova et al. (2017) state that geomagnetic pulsations detected during geomagnetically quiet

days can be related to substorms, which are periods of enhanced auroral activity characterized by sudden intensifications in the Earth's magnetic field. The authors investigated the parameters of auroral and geomagnetic pulsations in the frequency range of 1-4 mHz during quiet geomagnetic intervals preceding auroral substorms and non-substorm background variations. The study found that the power spectral density of these pulsations was higher during the pre-substorm intervals than during non-substorm days and that specific variations in pulsation parameters (substorm precursors) occurred during

the last 2-4 pre-substorm hours. Therefore, two pulses can occur during geomagnetically quiet days if substorms are present. To fully answer this question, we would need to investigate the behavior of magnetic substorms, which is beyond the scope of our article. We could identify pulses (red rectangles) between 15:00 UT and 16:00 UT due to the intense flow of matter from the Sun, which reaches a high intensity during this period. Also, the EEJ region amplifies the amplitudes of KOU and TTB data. Day 22 did not show any pulse greater than 0.2 nT in the SJG station, and the signal from KOU and SJG did not coincide. Day 23 did not present any pulse greater than 0.2 nT. Figure 11 shows the amplitudes and spectrogram of day 21. Between 7MHz and 15MHz, we find a 'belt' denoting the frequency range of the Pc4 pulse. The TTB station shows amplitudes near 0.5 nT due to the influence of the EEJ zone.

For disturbed days we found seven pulses in total for the period of 25, 26, and 27. Day 25 did not show any amplitude, filling the criteria to be a Pc4 pulse because the signal presented amplitudes smaller than 0.2 nT. The data of day 26 showed the minimum value for the Dst index, and the three pulses were identified between 12:00 UT and 14:00 UT (red rectangles in Figure 12), one pulse at SJG, one pulse at ARA, and one pulse at KOU. There are no data of TTB in this time interval. On day 27, we identified Pc4 pulses between 10:00 UT and 12:00 UT (red rectangles in Figure 12): one pulse at KOU station, one pulse at SJG station and one pulse at ARA station. Figures 14 and 15 show, respectively, the spectrograms of days 26 and 27. Day 26 shows a range between 9MHz and 15 MHz covering the Pc4 pulses where we could identify them isolated. Day 27 shows the same frequency range, but the spectrogram does not present the isolated Pc4 pulses. The SJG station presented a maximum amplitude of 0.198 nT, which we interpreted as a probable Pc4 pulse.
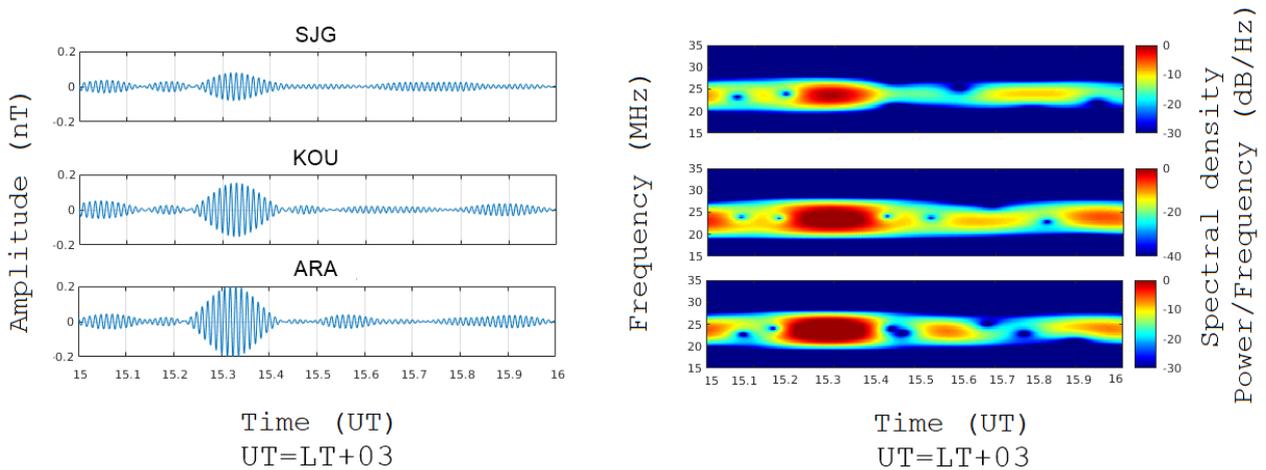

Figure 9: Identification of Pc3 pulses of KOU, SJG, and ARA stations on 27 August 2018 from 16:00 UT to 17:00 UT. Left: pulse amplitudes. Right: pulse spectrograms.
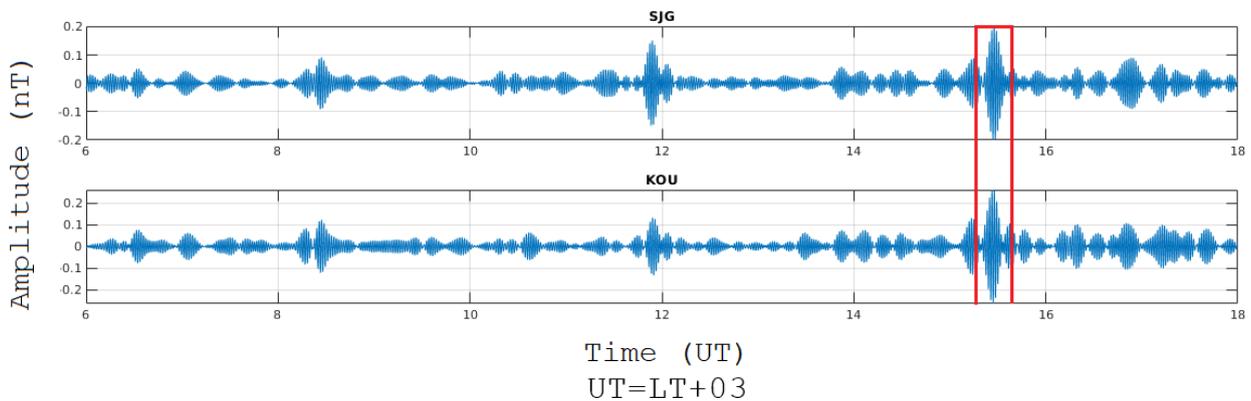

Figure 10: Pc4 identification on 21 August 2018. Red rectangles identify the pulses.
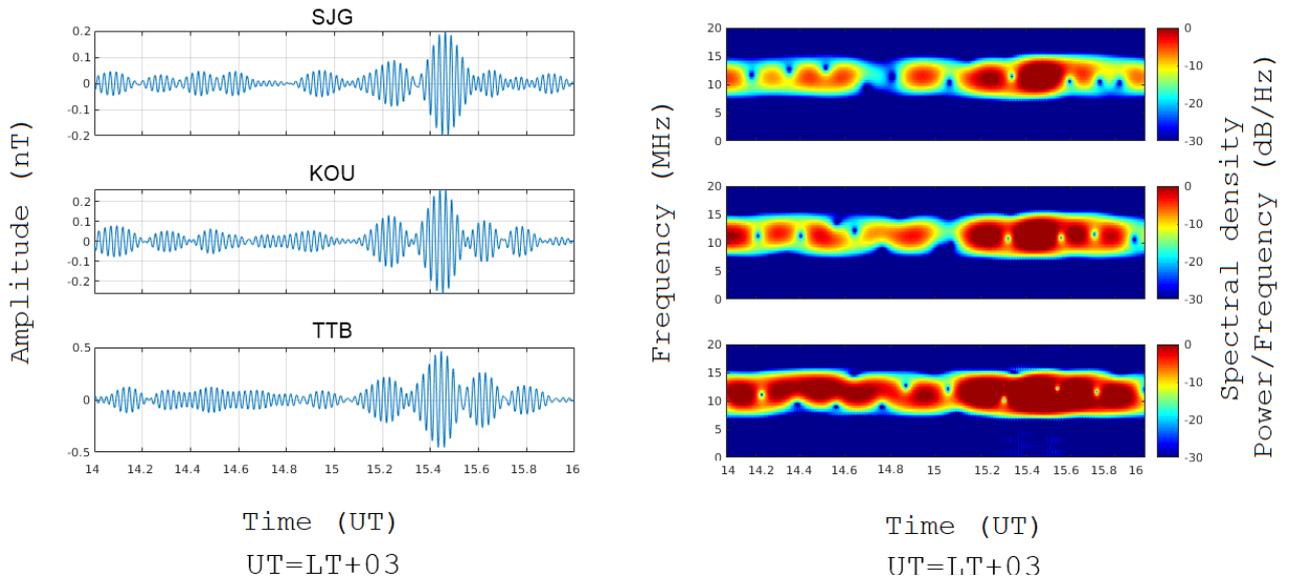
Figure 11: Identification of Pc4 pulses of KOU, SJG, and TTB stations 21 August 2018 from 14:00 UT to 16:00 UT. Left: pulse amplitudes. Right: pulse spectrograms.
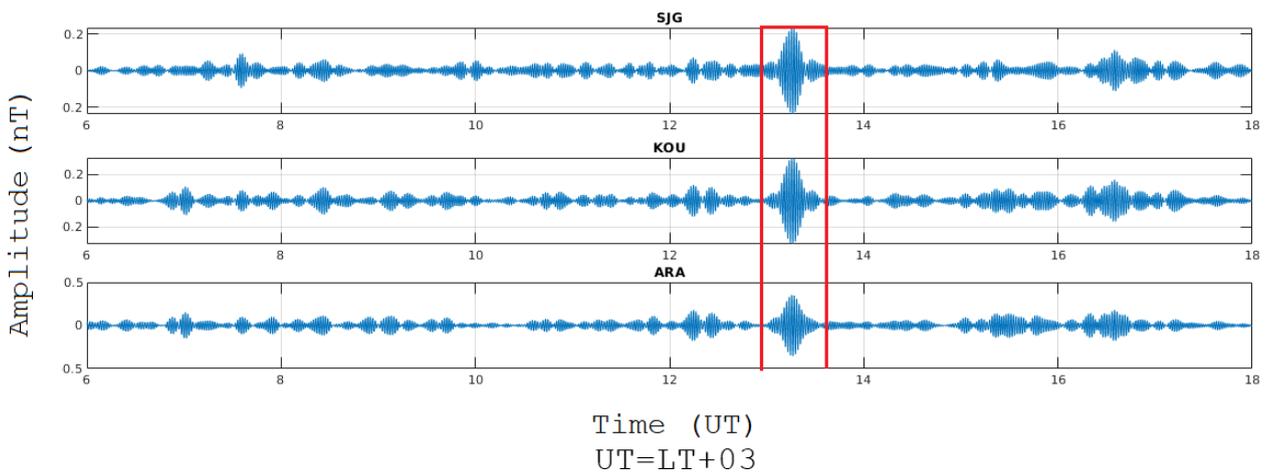

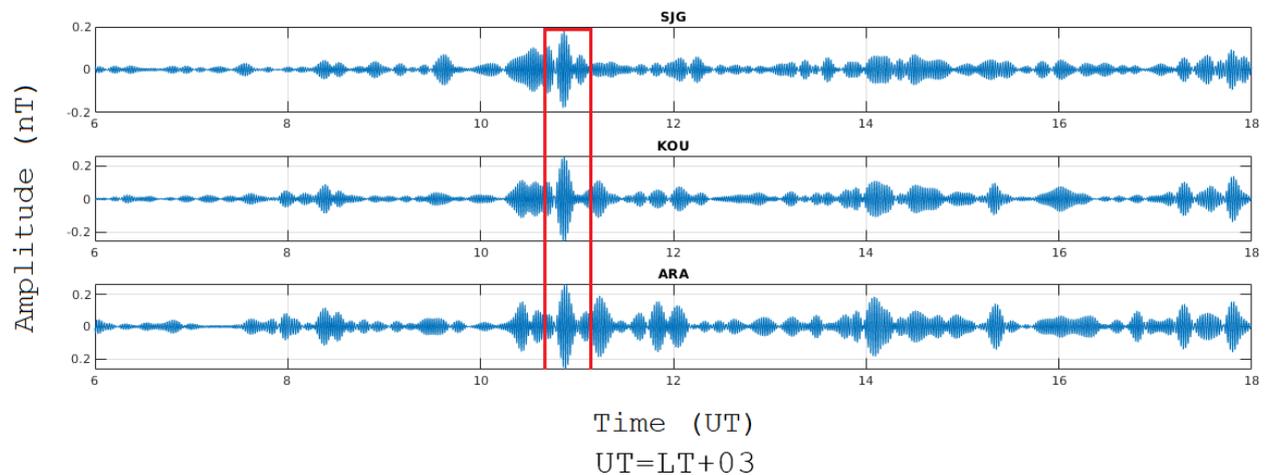Figure 12: Pc4 identification on 26 August 2018. Red rectangles identify the pulses.

Figure 13: Pc4 identification on 27 August 2018. Red rectangles identify the pulses.
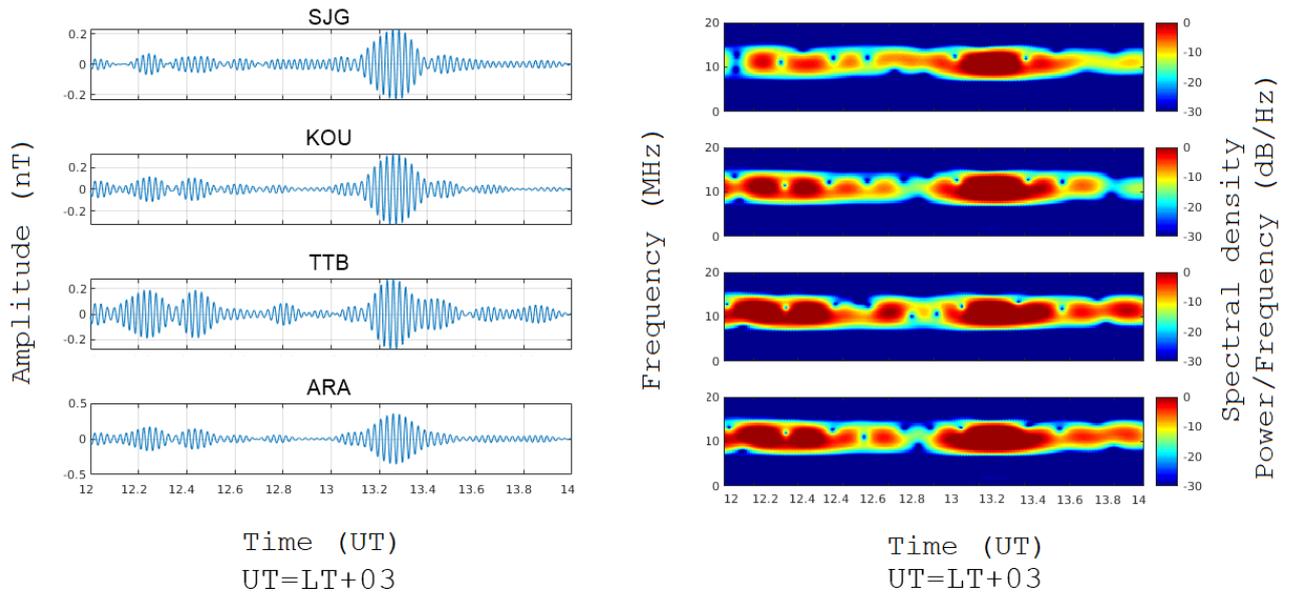
Figure 14: Identification of Pc4 pulses of KOU, SJG, ARA, and TTB stations on 26 August 2018 from 12:00 UT to 14:00 UT. Left: pulse amplitudes. Right: pulse spectrograms.
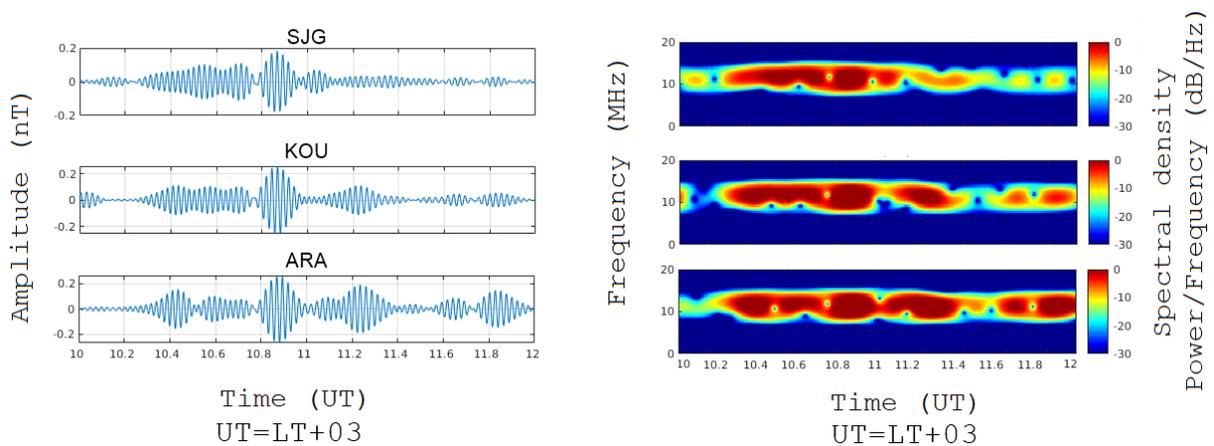

Figure 15: Identification of Pc4 pulses of KOU, SJG, and ARA stations on 27 August 2018 from 10:00 UT to 12:00 UT. Left: pulse amplitudes. Right: pulse spectrograms.

DISCUSSION

The behavior of Pc3 and Pc4 pulses is associated with the Cowling conductivity (Hughes and Southwood, 1976). To understand how conductivity works, it is necessary to understand the components of the ionospheric conductivity, considering the existence of two fields, the electric and the magnetic. The ionospheric conductivity is presented in terms of three components: horizontal component of the ionospheric magnetic field (σ_0), electric field vector perpendicular to the magnetic field (σ_1) and electric vector (σ_2) perpendicular to σ_0 and σ_1. The components are expressed as

$$\sigma_0 = Ne^2 \left[\frac{1}{m_e v_e} + \frac{1}{m_i v_i} \right], \tag{4}$$

$$\sigma_1 = Ne^2 \left[\frac{v_e}{m_e(v_e^2 + \Omega_e^2)} + \frac{v_i}{m_i(v_i^2 + \Omega_i^2)} \right], \tag{5}$$

$$\sigma_2 = Ne^2 \left[-\frac{\Omega_e}{m_e(v_e^2 + \Omega_e^2)} + \frac{\Omega_i}{m_i(v_i^2 + \Omega_i^2)} \right], \tag{6}$$

where subscript e denotes electron and i denotes ions, so v_e and v_i are the respective frequency of collision; Ω_e and Ω_i are the respective cyclotronic frequencies; m_e and m_i are the respective masses of the electrons and ions; N is the electronic density; and e is the electric charge (Itonaga et al., 1998).

The longitudinal conductivity (equation 4) describes the particles of the electronic charges along with the extension of the geomagnetic field in the presence of an electric field. When the electric field components are perpendicular to a magnetic field, the conductivity parallel to the current flow is defined as Pedersen conductivity (equation 5) and the conductivity orthogonal to the current flow is defined as Hall conductivity (equation 6). The Cowling conductivity, σ_c, is a function of all parameters mentioned, and it is defined as:

$$\sigma_c = \sigma_1 + \frac{\sigma_2^2}{\sigma_1}, \tag{7}$$

According to Roy and Rao (1998), there is not a unified answer in the literature about the origin of magnetic pulsations; however, Sarma and Sastry (1995) have stated that pulsations on the magnetic equator are related to the presence of a constant ionospheric current flow. Theories about the E-region of the ionosphere showed that the effects of amplitude variation of the pulses at the magnetic equator are a function of the Cowling conductivity (Kikuchi and Araki, 1979; Itonaga et al., 1998). The pulses are related to the upstream waves (generated by ionic cyclotron instabilities on the magnetosphere bow shock) that propagate along the equatorial region of the magnetosphere. The increase of Cowling conductivity in this latitude is responsible for the damping effect in the pulse signals.

This work represents a novel attempt to investigate the origin and behavior of aeronomic phenomena associated with variations in the geomagnetic activity. In order to achieve this, we conducted an analysis of magnetic data to identify and characterize geomagnetic pulses from four magnetic stations around the Amazon Region, which is an important region for equatorial phenomena. Table 3 summarizes the occurrences of Pc3 and Pc4 pulses observed in this study.

Table 3 - Summary of the geomagnetic pulsations observed during the period around the geomagnetic storm of 25th August 2018.

Pulse	21/08	22/08	26/08	27/08
Pc3	KOU TTB SJG ARA	KOU SJG	KOU TTB SJG ARA	KOU SJG ARA
Pc4	KOU TTB SJG		KOU TTB SJG ARA	KOU SJG ARA

CONCLUSIONS

We studied the behavior of Pc3 and Pc4 type pulsations on geomagnetically quiet and disturbed days. We used bandpass filtering and spectrograms to identify Pc3 pulsations and Pc4 on days 21, 22, 23, 25, 26, and 27 August 2018. In addition, we chose stations closer to the magnetic equator to characterize the effect of EEJ on these pulsations. The results may contribute to understanding the mechanism that changes the amplitudes of the signals detected in the region of the magnetic equator. For future investigations, we recommend using power density to quantify the amplification and damping of pulse amplitudes. Furthermore, the lack of coverage of stations in the Amazon decreased the details of the variation of pulsations, so we recommend the use of more data from the equatorial region.

ACKNOWLEDGMENTS

Data and Materials Availability

The data that support the findings of this study are available on request from the corresponding author.

REFERENCES

Aarons, J, 1991, The role of the ring current in the generation or inhibition of equatorial F layer irregularities during magnetic storms: Radio Science, **26(4)**, 1131-1149, doi: 10.1029/91RS00473.

Alken, P., Thébault, E., Beggan, C.D., Amit, H., Aubert, J., Baerenzung, J., Bondar, T.N., Brown, W.J., Califf, S., Chambodut, A., Chulliat, A., Cox, G.A., Finlay, C.C., Fournier, A., Gillet, N., Grayver, A., Hammer, M.D., Holschneider, M., Huder, L., Hulot, G., Jager, T., Kloss, C., Korte, M., Kuang, W., Kuvshinov, A., Langlais, B., Léger, J.-M., Lesur, V., Livermore, P.W., Lowes, F.J., Macmillan, S., Magnes, W., Mandea, M., Marsal, S., Matzka, J., Metman, M.C., Minami, T., Morschhauser, A., Mound, J.E., Nair, M., Nakano, S., Olsen, N., Pavón-Carrasco, F.J., Petrov, V.G., Ropp, G., Rother, M., Sabaka, T.J., Sanchez, S., Saturnino, D., Schnepf, N.R., Shen, X., Stolle, C., Tangborn, A., Tøffner-Clausen, L., Toh, H., Torta, J.M., Varner, J., Vervelidou, F., Vigneron, P., Wardinski, I., Wicht, J., Woods, A., Yang, Y., Zeren, Z., and Zhou, B., 2021, International Geomagnetic Reference Field: The thirteenth generation: Earth, Planets and Space, **73**, 1, 49, doi: 10.1186/s40623-020-01288-x.

Biermann, L., 1963,The plasma tails of comets and the interplanetary plasma: Space Science Reviews, Kluwer Academic Publishers, **v. 1**, n. 3, p. 553–553. ISSN 0038-6308, doi: 10.1007/BF00225271.

Campbell W.H., 2003, Introduction to Geomagnetic Fields: Cambridge University Press; 337p, doi: 10.1017/CBO9781139165136.

Chapman, S., and Bartels, J., 1940, Geomagnetism: Oxford University Press, Oxford. 1049 pp., doi: 10.2307/3606494

Chen, C.-H., Lin, J.-Y., Gao, Y., Lin, C.-H., Han, P., Chen, C.-R., Lin, L.-C., Huang, R., and Liu, J.-Y., 2021, Magnetic pulsations triggered by microseismic ground motion: Journal of Geophysical Research: Solid Earth, **126, 3**, e2020JB021416, doi: 10.1029/2020JB021416.

Denardini, C.M., Chen, S.S., Resende, L.C.A., Moro, J., Bilibio, A.V., Fagundes, P.R., Gende, M.A., Cabrera, M.A., Bolzan, M. J.A., Padilha, A.L., Schuch, N.J., Hormaechea, J.L., Alves, L.R., Barbosa Neto, P.F., Nogueira, P.A.B., Picanço, G. A.S., and Bertollotto, T.O., 2018, The Embrace Magnetometer Network for South America: Network description and its qualification: Radio Science, **53**, 288–302, doi: 10.1002/2017RS006477.

Dungey, J.W., 1961, Interplanetary Magnetic Field and the Auroral Zones: Phys. Rev. Lett., American Physical Society, **6**, 2, 47–48, doi: 10.1103/PhysRevLett.6.47.

Gonzalez, W.D.; Joselyn, J.A.; Kamide, Y.; Kroehl, H.W.; Rostoker, G.; Tsurutani, B.T., and Vasyliunas, V.M., 1994, What is a geomagnetic storm?: Journal of Geophysical Research, **99**, A4, 5771–5792, doi: 10.1029/93JA02867.

Hasegawa, A., and Chen, L., 1974, Plasma Heating by Alfvén-Wave Phase Mixing: Physical Review Letters, **32**, 454, doi: 10.1103/PhysRevLett.32.454.

Heyns, M.J., Lotz, S.I., and Gaunt, C.T., 2020, Geomagnetic Pulsations Driving Geomagnetically Induced Currents: Space Weather, **19**, e2020SW002557, doi: 10.1029/2020sw002557.

Hughes, W.J., and Southwood, D.J., 1976, The screening of micropulsation signals by the atmosphere and ionosphere: Journal of Geophysical Research, **81**, 19, 234–3240, doi: 10.1029/JA081i019p03234.

Itonaga, M., Yoshikawa, A., and Yumoto, K., 1998, Transient response of the nonuniform equatorial ionosphere to compressional MHD waves: J. Atmos. Sol.-Terr. Phys., **60**, 253-261, doi: 10.1016/S1364-6826(97)00110-7.

Jacobs, J.A., Kato, Y., Matsushita, S., and Troitskaya, V.A., 1964, Classification of geomagnetic micropulsations: J. Geophys. Res., **69**, 180–181, doi: 10.1029/JZ069i001p00180.

Kamide, Y., and Chian, A. 2007. Handbook of the Solar-Terrestrial Environment: Springer. Berlin, Germany. 539 pp, doi: 10.1007/978-3-540-46315-3.

Kanasewich, E.R., 1981, Time sequence analysis in geophysics. Edmonton: University of Alberta, Alberta, Canada. 492 pp, doi: 10.1093/gji/43.3.1026.

Kelley, M.C., 2009, The Earth´s Ionosphere: Plasma Physics and Electrodynamics: Academic Press, San Diego, USA. 576 pp, doi: 10.1126/science.248.4951.89.

Kikuchi, T., and Araki, T., 1979, Horizontal transmission of the polar electric field to the equator: Journal of Atmospheric and Terrestrial Physics, **41**, 9, 927–936, doi: 10.1016/0021-9169(79)90094-1.

Kivelson, M.G., and Russell, C.T., 1995, Introduction to space physics: Cambridge University Press. Cambridge, UK. 568 pp, doi: 10.1017/9781139878296.

Marchezi, J.P., 2016, Identificação de pulsações geomagnéticas detectadas na rede de magnetômetros de EMBRACE. Master Thesis. INPE. São José dos Campos, SP, Brazil.

Mcpherron, R.L., 2005, Magnetic Pulsations: their sources and relation to solar wind and geomagnetic activity: Surveys in Geophysics, **36**, 5, 545-592, 2005, doi: 10.1007/s10712-005-1758-7.

Moldwin, M.B., 2008, An Introduction to space weather: Cambridge University Press, Cambridge, UK. 134 pp, doi: 10.1017/CBO9780511801365.

Murphy, B.S., and Egbert, G.D., 2018, Source biases in midlatitude magnetotelluric transfer functions due to Pc3-4 geomagnetic pulsations: Earth, Planets and Space, **70**, 1, doi: 10.1186/s40623-018-0781-0.

Omondi, S., Yoshikawa, A., Zahra, W.K., Fathy, I., and Mahrous, A., 2022, Automatic detection of auroral Pc5 geomagnetic pulsation using machine learning approach guided with discrete wavelet transform: Advances in Space Research, **70**, 6, 1496–1507. 10.1016/j.asr.2022.06.063.

Okamura, S., 2011, The short time Fourier transform and local signals: Phd Thesis. Carnegie Mellon University, Pittsburgh. USA.

Parks, G.K., 1991, Physics of space plasmas: an introduction. Redwood City, CA: Addison-Wesley, California, USA. 538 p. 10.1201/9780429301674.

Patra, A.K., and Rao, N., 2006, Radar observations of daytime 150-km echoes from outside the equatorial electrojet belt over Gadanki: Geophysical Research Letters, **33**, L03104, doi: 10.1029/2005GL024564.

Piassi, A.R., 2018, Análise de pulsações magnéticas Pc3 e Pc4 na região da anomalia magnética do Atlântico Sul: Master Thesis. INPE, São José dos Campos, SP, Brazil.

Roy, M., and Rao, D.R.K., 1998, Frequency dependence of equatorial electroject effect on geomagnetic micropulsations: Earth, Planets and Space, **50**, 10, p. 847–851, doi: 10.1186/BF03352178.

Samson, J.C., 1991, Chapter 6: Geomagnetic pulsations and plasma waves in the Earth's magnetosphere, *in* Jacobs, J. A. (ed.). Geomagnetism: London Academic Press, London, UK. p. 481–592. [10.1016/B978-0-12-378674-6.50012-1](10.1016/B978-0-12-378674-6.50012-1).

Saito, T., 1969, Geomagnetic pulsations. Space Science Reviews, **10**, 3, 319–412, doi: [10.1007/BF00203620](10.1007/BF00203620).

Sarma, S.V.S., and Sastry, T.S., 1995, On the equatorial electrojet influence on geomagnetic pulsation amplitudes: Journal of Atmospheric and Terrestrial Physics, **57**, 7, 749-754, doi: [10.1016/0021-9169(94)00053-Q](10.1016/0021-9169(94)00053-Q).

Schunk, R.W., and Nagy, A.F., 2009, Ionospheres: physics, plasma physics, and chemistry: 2. ed Cambridge University Press, Cambridge, UK. 628 pp, doi: [10.1017/CBO9780511635342](10.1017/CBO9780511635342).

Shinoraha, M., Hosen, Y., Yoshikawa, A., Tachihara, H., Saka, O., and Kitamura, T.I., 1998, Wave characteristics of geomagnetic pulsations across dip equator: Journal of Geophysical Research, **103**, A6, doi: [10.1029/97JA03067](10.1029/97JA03067).

Sibeck, D.G., 1994, Transient quasi-periodic (5 - 15 min) events in the outer magnetosphere, *in* Engebretson, M. J.; Takahashi, K.; Scholer, M. (eds.) Solar wind sources of magnetospheric ultralow-frequency waves: AGU Geophysical Monography, **81**, Washington DC, USA. p.173–182.

Silva, G.B.D., 2017, Caracterização da amplitude de pulsações magnéticas observadas em região sob influência do eletrojato equatorial: Master Thesis. INPE. São José dos Campos, SP, Brazil.

Yagova, N., Nosikova, N., Baddeley, L., Kozyreva, O., Lorentzen, D.A., Pilipenko, V., and Johnsen, M.G., 2017, Non-triggered auroral substorms and long-period (1–4 mHz) geomagnetic and auroral luminosity pulsations in the polar cap: Annals of Geophysics, **35**, 365–376, doi: 10.5194/angeo-35-365-2017.

Yagova, N.V., Pilipenko, V.A., Sakharov, Y.A., and Selivanov, V.N., 2021, Spatial scale of geomagnetic Pc5/Pi3 pulsations as a factor of their efficiency in generation of geomagnetically induced currents: Earth, Planets and Space, **73**, 1, doi: [10.1186/s40623-021-01407-2](10.1186/s40623-021-01407-2).

Youngworth, R. N., Gallagher, B. B., and Stamper, B. L., 2005, An overview of power spectral density (PSD) calculations, *in* Optical Manufacturing and Testing VI, **vol. 5869**, p. 58690U. International Society for Optics and Photonics, doi: [10.1117/12.618478](10.1117/12.618478).